Synchronization and firing death in the dynamics of two interacting excitable units with heterogeneous signals

D. Hennig and L. Schimansky-Geier
Institut für Physik, Humboldt-Universität Berlin, Newtonstrasse 15, 12489 Berlin, Germany
(Received 29 May 2007; published 13 August 2007)

We study the response of two coupled FitzHugh-Nagumo systems to heterogeneous external inputs. The latter, modeled by periodic parametric stimuli, force the uncoupled excitable systems into a regime of chaotic firing. Due to parameter dispersion involved in randomly distributed amplitudes and/or phases of the external forces the units are nonidentical and their firing events will be asynchronous. Interest is focused on mutually synchronized spikings arising through the coupling. It is demonstrated that the phase difference of the two external forces crucially affects the onset of spike synchronization as well as the resulting degree of synchrony. For large phase differences the degree of spike synchrony is constricted to a maximal possible value and cannot be enhanced upon increasing the coupling strength. We even found that overcritically strong couplings lead to suppression of firing so that the units perform synchronous subthreshold oscillations. This effect, which we call "firing death," is due to a coupling-induced modification of the excitation threshold impeding spiking of the units. In clear contrast, when only the amplitudes of the forces are distributed perfect spike synchrony is achieved for sufficiently strong coupling.

DOI: 10.1103/PhysRevE.76.026208 PACS number(s): 05.45.Xt, 05.40.−a, 87.18.Sn, 82.40.Bj

I. INTRODUCTION

The phenomenon of synchronization of coupled oscillators occurs in various fields [1–6]. With the observation of synchronous firing of neurons [7,8], which is assumed to play a vital role for the information processing and coding in the brain, the investigation of synchronization of coupled units in the realm of neuroscience has attracted renewed interest.

To understand the underlying mechanisms of the nonlinear dynamics of neural units that lead to complex neuron activities such as synchronous, asynchronous, and chaotic firing behavior studying the response of interacting neurons to external inputs is indispensable [9,10]. Particularly for encoding external signals synchronization provides a possible mechanism [11]. Neuronal activity is reflected in a significant departure of the electrical cross membrane potential of the neuron from its quiescent state which is caused by a stimulus above a certain threshold in amplitude. This generates a spike that decays back to quiescence during a refractory period in which further spike generation is inhibited [12]. This feature is typical for an excitable system. A model of an excitable media is represented by the FitzHugh-Nagumo (FHN) system [13,14] which is widely used as a simplified version of the Hodgkin Huxley system [15] in neuroscience to study neural activities as nonlinear phenomena. In the frame of the FHN model neuronal excitability is described by a two-dimensional relaxation oscillator. A small but finite perturbation away from a steady state results in a large excursion followed by a refractory period at the end of which the system returns to the steady state. With appropriate changes of the excitability parameter or with external inputs it is also possible to evoke in the (excitable) FHN system an oscillatory regime where it exhibits repetitive firings consisting of a train of spikes.

The response of a spontaneously oscillating system to external periodic drivings involves entrainment for certain values of the amplitude and frequency of the perturbation, quasiperiodicity, and chaos [16–23]. Such qualitatively distinct behavior plays a role in many systems with biological, chemical, and physical backgrounds [24].

Our study deals with the stimulation of relaxation oscillations in the coupled dynamics of two activator-inhibitor units. The purpose is to understand the implications of the width and amount of parameter heterogeneity in the external stimuli on the synchronization features of two coupled chaotic units. To be precise, we focus interest on mutually synchronized spikings when the parameters of the external drivings are chosen such that through the locally acting periodic forces each (uncoupled) unit is brought into a regime of chaotic spiking. Moreover, due to the parameter dispersion the units are nonidentical and hence, if uncoupled, the firing events (even for identical initial conditions) of the units will be asynchronous leading to a distribution of the spiking times.

In the field of neurodynamics networks consisting of coupled excitable and oscillatory units have been investigated with view to the synchronization features [25–28]. Concerning the role of heterogeneity it has been demonstrated that diversity may even promote the instigation of global oscillations in a heterogeneous excitable medium [29].

The key question that arises in our study then is: For which extent of parameter dispersion, do completely synchronous oscillations of the coupled units arise? In previous studies, it has been argued that in certain systems of coupled chaotic oscillators the oscillations become less and less incoherent with increasing coupling strength and eventually complete synchronization is accomplished [10,30–34]. On the other hand, it has been demonstrated that beyond a certain coupling strength units within an oscillatory network can reciprocally suppress their oscillations, dubbed "oscillation death" [35]. The aim of our study is also to elucidate how the coupling strength influences the synchronization of two

coupled chaotic oscillators with a distribution of their local driving terms.

The paper is organized as follows: In the next section we introduce the model of the two coupled FHN units and present a proof of complete synchronization. Afterwards the interaction of two chaotically spiking units is studied where attention is paid to the combined influence of the coupling strength and parameter dispersion on the synchronization behavior. It is shown that the difference in the phases of the parametric drivings has strong impact on synchrony. Finally we summarize our results.

II. THE DRIVEN COUPLED FHN MODEL

We study the dynamics of two coupled FHN oscillators obeying the following set of equations:

$$\dot{x}_1 = \frac{1}{\epsilon}[x_1 - x_1^3 - y_1] + \kappa[x_2 - x_1], \tag{1}$$

$$\dot{y}_1 = \gamma x_1 - \beta y_1 + b + s_1(t) y_1, \tag{2}$$

$$\dot{x}_2 = \frac{1}{\epsilon}[x_2 - x_2^3 - y_2] + \kappa[x_1 - x_2], \tag{3}$$

$$\dot{y}_2 = \gamma x_2 - \beta y_2 + b + s_2(t) y_2, \tag{4}$$

where x_n and y_n $(n=1,2)$ refer to the activator (voltage) and inhibitor (recovery) variable, respectively. Coupling extends among the activator variables (electrical coupling). κ denotes the coupling strength. The time separation between the fast activator and slow inhibitor variable, respectively, is determined by the small quantity ϵ. Each unit is subjected to an external stimulus (current) $s_n(t)$ which is supposed to be sinusoidal

$$s_n(t) = -A_n \cos(\Omega_n t + \phi_n^0) \tag{5}$$

and forces parametrically the corresponding inhibitor variable. Periodic forcing of the inhibitor variables in FHN systems was also considered in Ref. [36]. The amplitudes A_n, frequencies Ω_n, as well as phases ϕ_n^0 can be distributed in some range. This is where heterogeneity enters in our model. Thus our model system consists of two coupled nonidentical FHN units. The parameter β in Eqs. (2) and (4) determines the relaxation of the ionic concentration y when elevated from its equilibrium level. Elevations are due to the opening of ion stores regulated by ion channels. These are sensitive to membrane variations the impact of which we attribute to the last term in Eqs. (2) and (4) to time-dependent modulations of the parameter β (also see Ref. [37]).

A. Complete synchronization

Here we prove the following synchronization theorem.

Theorem. Two coupled FHN units obeying Eqs. (1)–(4) completely synchronize asymptotically and exponentially fast irrespective of the initial conditions provided that the following constraint is fulfilled:

$$\kappa > \frac{1}{4}\left[\frac{3}{\epsilon} + \gamma + 2(A-\beta)\right], \tag{6}$$

where $A>0$ denotes the amplitude of the equal driving force $s_1(t)=s_2(t)=-A\cos(\Omega t+\phi^0)$.

Proof. The proof proceeds by showing that distance between the two trajectories $d=\sqrt{(x_2-x_1)^2+(y_2-y_1)^2}$, serving as the synchronization measure, approaches asymptotically zero. One gets

$$\begin{aligned}\frac{1}{2}\frac{d}{dt}d^2 = d\dot{d} = (x_2-x_1)\{[(x_2-x_1)-(x_2^3-x_1^3)-(y_2-y_1)]/\epsilon \\ - 2\kappa(x_2-x_1)\} + (y_2-y_1)[\gamma(x_2-x_1) - \beta(y_2-y_1) \\ + (s_2y_2 - s_1y_1)].\end{aligned} \tag{7}$$

With the help of $(x_2-x_1)^2-(x_2-x_1)(x_2^3-x_1^3)\le(x_2-x_1)^2$ we get the following bounds for the right-hand side (RHS) of Eq. (7):

$$\begin{aligned}d\dot{d} \le \frac{1}{\epsilon}[(x_2-x_1)^2 - (x_2-x_1)(y_2-y_1)] - 2\kappa(x_2-x_1)^2 \\ + \gamma(x_2-x_1)(y_2-y_1) + (A-\beta)(y_2-y_1)^2.\end{aligned} \tag{8}$$

Expressing the terms on the RHS in polar coordinates

$$x_2 - x_1 = d\cos\Theta, \quad y_2 - y_1 = d\sin\Theta, \tag{9}$$

with $\Theta\in[0,2\pi)$ we obtain

$$\begin{aligned}d\dot{d} \le \left[\frac{1}{\epsilon}\cos^2\Theta + \left(\gamma - \frac{1}{\epsilon}\right)\cos\Theta\sin\Theta + (A-\beta)\sin^2\Theta\right]d^2 \\ - 2\kappa d^2\cos^2\Theta.\end{aligned} \tag{10}$$

Finally, with the relations $|\cos\Theta\sin\Theta|\le 1/2$, $|\cos^2\Theta|\le 1$, and $|\sin^2\Theta|\le 1$ we arrive at the equation expressed in the radial variable

$$\dot{d} \le (\alpha - 2\kappa)d, \tag{11}$$

where we introduced the abbreviation

$$\alpha = \frac{3}{2\epsilon} + \frac{\gamma}{2} + A - \beta. \tag{12}$$

Consequently, solutions of the system

$$\dot{u} = (\alpha - 2\kappa)u \tag{13}$$

form an upper bound for $d(t)$ in the sense that $0\le d(t)\le u(t)$. $u(t)$ decays exponentially in time, i.e., $u(t)=u(0)\exp(-\lambda t)$, provided the inequality

$$\lambda \equiv \alpha - 2\kappa < 0 \tag{14}$$

holds. From the last inequality we infer that the relation

$$\kappa > \frac{1}{4}\left(\frac{3}{\epsilon} + \gamma + 2(A-\beta)\right) \tag{15}$$

guarantees that λ is always negative which concludes the proof. Exponential decay of $d(t)$ ensures that the synchronized state is attained exponential fast.

From the inequality (15) we deduce that the more pronounced the activator-inhibitor time scale separation is, i.e.,

the smaller ϵ, the larger the critical coupling strength that is necessary to ensure synchronization. Notice that the expression for the critical coupling strength in Eq. (15) is independent of the frequency and phase of the parametric forces because merely their maximal amplitude A enters there. We remark that the theorem does not state whether one finds the system synchronized with the units in the regime of a steady state or subthreshold oscillations or suprathreshold relaxation oscillations. One cannot infer whether the synchronized motion is regular or in the chaotic regime. The relation (15) is of relevance for the forthcoming investigations as it gives evidence how the coupling strength κ affects synchronization.

III. TWO COUPLED FHN SYSTEMS

Before we embark on the study of the coupled dynamics we consider briefly a single driven FHN system

$$\dot{x} = \frac{1}{\epsilon}[x - x^3 - y], \tag{16}$$

$$\dot{y} = \gamma x - \beta y + b - A\cos(\Omega t + \phi^0)y. \tag{17}$$

Throughout the paper we fix the parameters as follows: $\epsilon=0.01$, $b=0.6$, $\beta=1$, $\gamma=1.5$, so that the undriven system of $A=0$ is in the excitable regime, i.e., there exist a unique attractive rest point (x_0,y_0) and a thresholdlike behavior for firing of the activator variable. More precisely, for subthreshold excitations away from the unique attractive equilibrium the latter is ultimately approached whereas for suprathreshold excitations a large amplitude excursion in phase space results being associated with a spike in the activator evolution.

A. Single driven FHN system

As far as the response of the unit to the periodic stimulus for $A \neq 0$ is concerned, different qualitative behavior is found depending on the choice of the parameters of the driving term. In this study we consider fixed frequency $\Omega=12$ and treat the amplitude A as the bifurcation parameter. The effect of parameter changes is seen in Fig. 1 where we show the bifurcation diagram of a single driven FHN system generated from a stroboscopic plot at successive periods of the driving force $T=2\pi/\Omega$. Initially the FHN system is situated at the single attracting equilibrium point. Under parametric forcing with low amplitudes there result small subthreshold oscillations around the attractive fixed point. That is a supercritical Hopf bifurcation takes place giving birth to a limit cycle with nearly harmonic oscillations. Further increase of A results in weak growth of the amplitude of the oscillations. As the driving strength passes through the critical value $A \simeq 0.59$ the amplitude of the oscillations suddenly rises significantly over an exponentially small range of the parameter A. That is large amplitude relaxation oscillations (spikes) are produced [38]. Upon further increase of the parameter A the amplitude of the limit cycle remains constant. This rapid change from small amplitude limit cycle oscillations to large ones is called the Canard phenomenon [38]. In our case the relaxation oscillations the period of the large amplitude relaxation

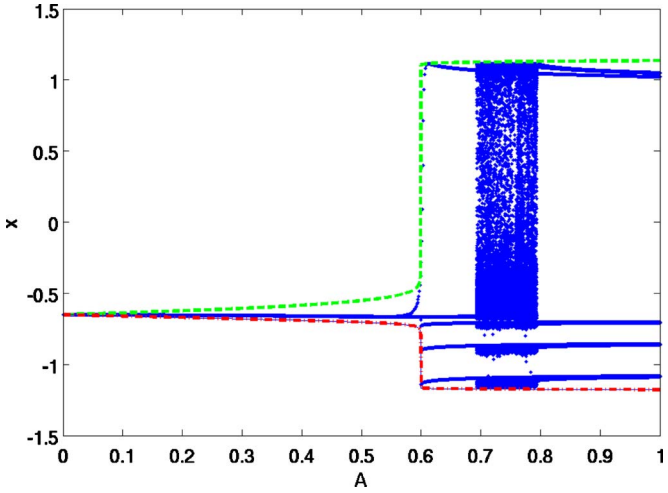

FIG. 1. (Color online) Bifurcation diagram of the rest state in dependence of the amplitude of the driving force for a single driven FHN system. The green dashed (red dashed dotted) line represents the maximum (minimum) of the activators' amplitudes. Parameters: $\epsilon=0.01$, $b=0.6$, $\beta=1$, $\gamma=1.5$, $\Omega=12$, and $\phi^0=0$.

oscillations is five times that of the periodic force. Between $A=0.7$ and 0.79 there is a band of chaotic solutions corresponding to aperiodic spike trains. The intervals between two successive spikes are characterized by small-amplitude (subthreshold) oscillations. More precisely, the system is excitable and possess a single stable rest state in form of a small-amplitude (subthreshold) limit cycle. The occurrence of the spikes is correlated with the periodic modification of the inhibitor nullcline according to $y=(\gamma x-b)/[\beta+s(t)]$. The driving term shifts the fixed point further away [if $s(t)>0$] or closer to [if $s(t)<0$] the effective excitation threshold. Thus near the maximum of the external force spiking becomes more likely.

Increasing the amplitude beyond $A=0.79$ restores regularity and renders the system oscillatory, i.e., periodic large-amplitude oscillations along a limit cycle are generated being entrained to the external forcing. As illustrated in Fig. 2 chaotic spiking behavior is obtained when the phase of the external driving is varied in the range $\phi^0 \in [0,2\pi)$ and the amplitude is held fixed at $A=0.73$. Figure 1 shows that for this amplitude and a phase $\phi^0=0$ the dynamics is chaotic. In general, chaotic evolution is encountered for amplitudes lying in the interval $A \in [0.70,0.79)$ no matter how the phase is chosen which is verified by a corresponding positive maximal Lyapunov exponent. Figure 3 shows examples of chaotic and regular spike trains.

B. Two coupled driven FHN systems

We now consider the dynamics when two driven FHN units, where each of them for itself is in the chaotic spiking regime, get coupled.

1. Stroboscopic plots

To illustrate the complexity of the coupled dynamics stroboscopic plots of the activator variables $x_{1,2}$ as a function of

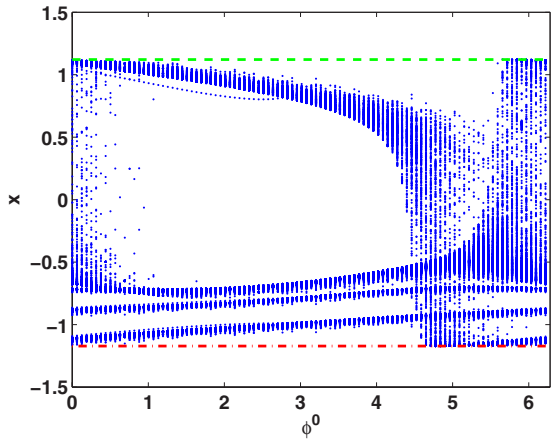

FIG. 2. (Color online) Bifurcation diagram of the rest state for a single driven FHN system as a function of the phase of the driving force $\phi^0 \in [0, 2\pi)$ for an amplitude $A=0.75$. Remaining parameters and assignment of the line types as in Fig. 1.

the coupling strength κ are depicted in Fig. 4. The pair of amplitudes $A_{1,2}$ of the driving force was chosen randomly from the interval of equally distributed amplitudes $A_n \in [0.70, 0.79]$. Additionally the phases are also taken as

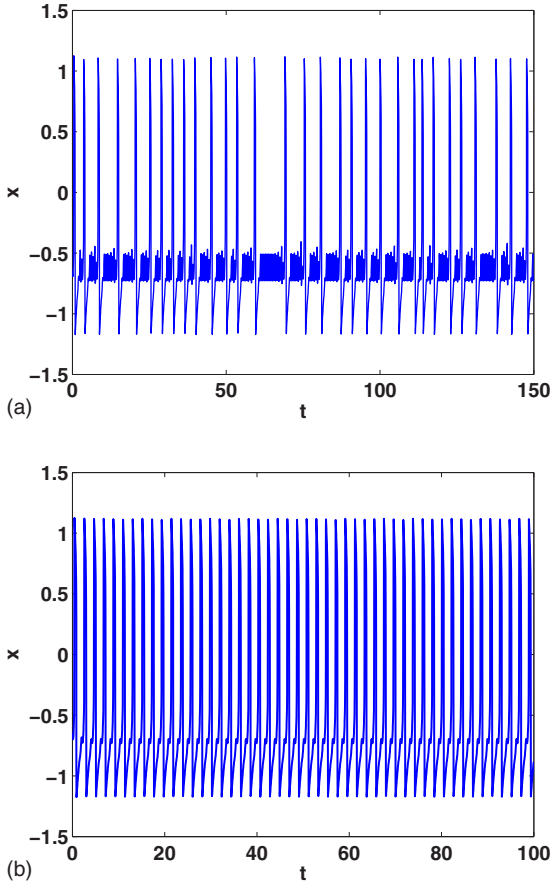

FIG. 3. (Color online) Time evolution of the activator variable $x(t)$. (a) Chaotic dynamics in the excitable regime. Amplitude of the periodic driving force $A=0.73$ remaining parameters as in Fig. 1. (b) Large-amplitude oscillations showing entrainment to the periodic driving force with amplitude $A=0.81$.

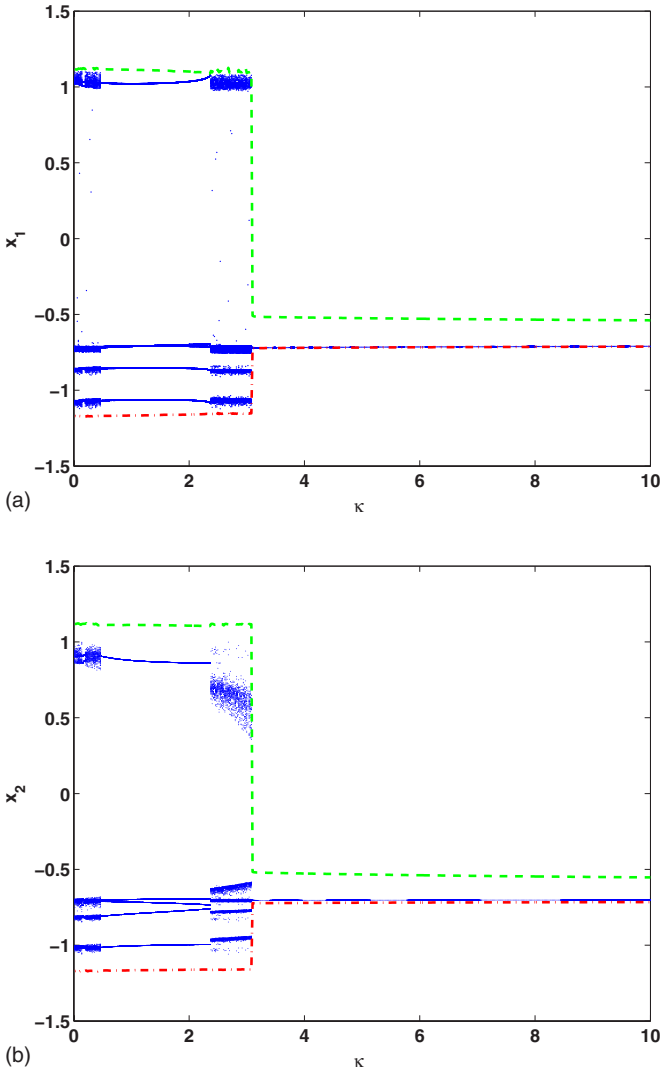

FIG. 4. (Color online) Stroboscopic plot for two coupled FHN units showing the activator variable x_1 (a) and x_2 (b) as a function of the coupling strength κ. The two driving amplitudes and phases were chosen at random from the intervals $A \in [0.7, 0.79]$ and $\phi \in [0, 2\pi)$ respectively with values $A_1=0.757$, $A_2=0.780$, $\phi_1^0=3.969$ and $\phi_2^0=5.559$. Remaining parameters and assignment of line style as in Fig. 1.

random from the range of equally distributed values $\phi_n^0 \in [0, 2\pi)$. In what follows we differentiate between two cases of parameter heterogeneity in the forcing term.

(i) When the amplitudes $A_{1,2}$ and phases $\phi_{1,2}^0$ are chosen at random from the interval $[0.70, 0.79]$ and $[0, 2\pi)$ respectively, which is referred to as forcing with random amplitudes and random phases, and

(ii) As in (i) but with fixed phases $\phi_{1,2}^0 = \phi^0$, which is referred to as forcing with only random amplitude.

Obviously, the amount of parameter heterogeneity is higher in (i) than in (ii). We report also briefly on the case of forcing with fixed equal amplitudes and random phases. In the first example shown in Fig. 4, as one realization of the random amplitudes and phases, the two coupled FHN units still spike

repetitively for $\kappa<3.08$. Furthermore in the range $0\leq\kappa<0.46$ and $2.38\leq\kappa\leq3.08$ the dynamics is chaotic while in between these two chaotic bands phase locking to the periodic stimulation is observed. Notably for $\kappa>3.08$ spiking gets annihilated due to the coupling and the dynamics exhibits only small amplitude oscillations that are entrained to the periodic forcing. Moreover, the two coupled oscillators evolve synchronously and the amplitudes of these oscillations are not affected by changes of the coupling strength (at least in the interval $3.08<\kappa\leq10$). This behavior (albeit small amplitude oscillations prevail in our case) is reminiscent of oscillation death where the return of the dynamics of coupled FHN units to the quiescent regime is induced by the coupling [35]. Since in our case the coupling-induced transition proceeds from large-amplitude excitations to small-amplitude oscillations around the quiescent state we call it "firing death." For later use we quote here the differences of the driving forces' amplitudes $A_1-A_2=-0.023$ and phases $\phi_1^0-\phi_2^0=-1.621$. The occurrence of the firing death can be explained on the basis of the excitability property of the coupled FHN units. Let us recall that for strong time scale separation the solution of the system (16) and (17) spends most of its time close to slow manifolds $S_{1,2}$ that is determined by the activator nullclines

$$S_1: y_1 = x_1 - x_1^3 + \epsilon\kappa(x_2 - x_1) \tag{18}$$

and

$$S_2: y_2 = x_2 - x_2^3 + \epsilon\kappa(x_1 - x_2). \tag{19}$$

Only for appropriate and strong enough perturbations can the solution be moved away from the stable rest state on one branch of $S_{1,2}$. Apart from $S_{1,2}$ the solution is then well approximated by straight lines $y_n=$const until it gets close to the other branch of $S_{1,2}$. The solution follows this part of $S_{1,2}$ until a critical point close to the local maximum is reached where the solution leaves $S_{1,2}$ again to re-approach in a straight line the starting branch of $S_{1,2}$. Thus escaping from $S_{1,2}$ is vital for the instigation of a large-amplitude excitation oscillation, i.e., a firing event. As noted above the excitation threshold is overcome when the external forces $s_{1,2}(t)$ pass through their maximum which triggers the solution in the region to the right of $S_{1,2}$. In Fig. 5 we depict a projection of the solution on the x_1-x_2 plane. The direction of rotation proceeds clockwise. Notice the strong asymmetry of the x_1-x_2 orbit due to the triggering of the subthreshold oscillations by the external forces with markedly different phases. We indicate those values of the activator variables for which the solution is beneath the slow manifolds $S_{1,2}$, i.e., for which

$$y_1(t) - [x_1(t) - x_1^3(t) + \epsilon\kappa(x_2 - x_1)] < 0 \tag{20}$$

$$y_2(t) - [x_2(t) - x_2^3(t) + \epsilon\kappa(x_1 - x_2)] < 0. \tag{21}$$

For the instigation of firing the solution needs to be beneath $S_{1,2}$ because only then the activator variables $x_{1,2}$ lie in the region where $\dot{x}_{1,2}>0$. Then the trajectory can undergo large phase space excursions to the right branch of the activator nullclines $S_{1,2}$. From the figures one infers that when the activator variables reach their maximum (and are about

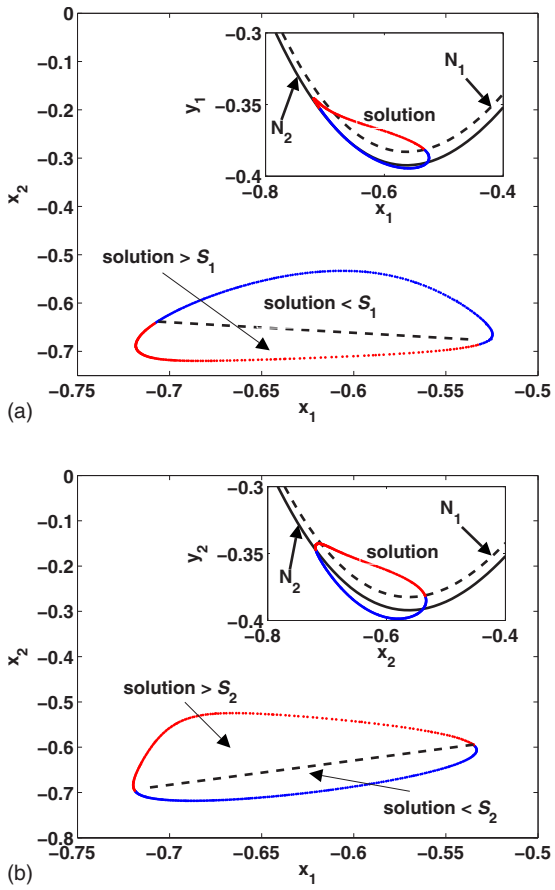

FIG. 5. (Color online) Projection of the solution on the x_1-x_2 plane with parameters as in Fig. 4 except for fixed coupling strength $\kappa=5$. The dashed line separates those ranges for which the solution lies beneath (red), respectively, above (blue) the slow manifold $y_1=x_1-x_1^3+\epsilon\kappa(x_2-x_1)$ (a) and $y_2=x_2-x_2^3+\epsilon\kappa(x_1-x_2)$ (b). The inset in (a) shows the projection of the solution on the x_1-y_1 plane together with the nullclines N_1 and N_2 for fixed values of x_2. The former (latter) corresponds to the case when the activator variable x_2 attains its maximum −0.533 (minimum −0.720). Likewise in the inset in (b) except that the x_2-y_2 projection of the nullclines N_1 and N_2 belong to the minimum and maximum of the x_1 variable, respectively.

to depart from $S_{1,2}$ to overcome the excitation threshold) the solution turn immediately to enter the region for which it comes to lie above the slow manifold. This is due to the fact that the large phase shift between the two activator variables in combination with a fairly large coupling strength κ contributes to large coupling terms $\epsilon\kappa(x_2-x_1)$ and $\epsilon\kappa(x_1-x_2)$. As a result the slow manifold gets such deformed that the excitation threshold is effectively shifted toward larger activator amplitudes. Notably the position and radius of the small-amplitude limit cycle are virtually unaffected by the coupling term. Thus overcoming the excitation threshold is inhibited. This feature is illustrated in the insets in Fig. 5 where the projections of the solution on the x_1-y_1 plane together with the nullclines $y_1=x_1-x_1^3+\epsilon\kappa(x_2-x_1)$ for two fixed values of $x_2(t)$ are displayed [(a)]. In the case of the nullcline labeled as N_1 the variable x_2 is fixed at its minimal −0.533 value while N_2 is drawn at maximal $x_2=-0.720$. Thus, N_1 and N_2

restrict the range within which the nullcline $y_1=x_1-x_1^3+\epsilon\kappa(x_2-x_1)$ experiences deformations induced by the dynamical changes of $x_2(t)$. (Equivalently, the inset in the lower panel characterizes the behavior on the x_2-y_2 plane.) Apparently, the solution remains trapped on the small-amplitude limit cycle.

Contrary to this behavior the dynamics for another random choice of the amplitudes and phases of the driving term suprathreshold oscillations are maintained and spiking is supported in the entire range of coupling strengths. The corresponding stroboscopic plots are contained in Fig. 6. For $\kappa \gtrsim 7$ the two activator variables perform mutually synchronous motions. Again we quote the differences of the driving forces' amplitudes $A_1-A_2=-0.003$ and phases $\phi_1^0-\phi_2^0=-0.016$.

2. Degree of spike synchrony

To quantify how synchronous the firing of the coupled units occur we use as a measure of spike synchrony the cross-correlation between spikes [39,40]. This method is based on the generation of trains of square pulses from the activator signal. To this end a pulse of height unity was placed on the time axis at moments of firing (i.e., when the activator variable exceeds a certain value with definite sign of its derivative) such that the latter constitute the center of the pulse. The width of a pulse was taken as 20% of the smallest firing period. Obtaining the cross-correlation of the pulse trains is equivalent to computing the area that is shared between the pulses associated with the two units. The degree of spike synchrony is then evaluated as the sum of the shared areas divided by the square root of the product of the total areas of each individual pulse train. Clearly, full asynchrony yields measure zero while perfect spike synchrony corresponds to measure unity. We emphasize that synchrony in the sense defined above relies on the simultaneous firing events of coupled units. This has to be distinguished from the synchrony measure used in the theorem of complete synchronization in Sec. II which puts a stronger request on the dynamics meaning that the difference between two neighboring trajectories vanishes asymptotically which does not necessarily involve that the coupled units spike at all. In what follows we refer to spike synchrony simply as synchrony.

The computation of the degree of synchrony is performed for an interval of 200 time units involving at least 25 spike events. For low coupling strength $\kappa<1$ the beginning of the interval is taken after a sufficient long time after the switch-on of the coupling so that contributions of transients are omitted. For moderate and strong coupling $\kappa \geq 1$ the synchronized state of coherent spiking is attained almost instantaneously. In Fig. 7 the synchrony measure versus coupling strength associated with the coupled dynamics in Figs. 4 and 6 is shown. Only in the coupling range when the spiking dynamics is chaotic one finds synchronous behavior. Suppression of (complete) spike synchrony in the phase-locked regime is due to the fact that the motion of the two FHN units is actually out-of-phase as it is the case in the coupling range $0.46<\kappa \lesssim 2.38$ in Fig. 4. In some intervals the degree of synchrony possesses a sensitive dependence on the coupling strength [see Fig. 7(b) for $\kappa \leq 4.9$] so that the corresponding graph has a complex structure. There are values of κ for which a fairly high degree of synchrony is found whereas for slightly deviating couplings the dynamics can be significantly less synchronous if not completely asynchronous. This sensitivity of the synchrony feature with respect to the coupling strength can be found on finer and finer scales on the κ axis which is characteristic of a fractal structure. Interestingly, for the case illustrated in Fig. 7(b), almost complete synchrony, i.e., the dynamics of the two systems is identical at any moment of time, is accomplished for $\kappa \gtrsim 7$ even though the dynamics is irregular. An example of the temporal behavior of chaotic synchronization of two coupled units is seen in Fig. 8. Notice that after the switch-on of the coupling of moderate strength $\kappa=1$ the synchronized state is almost instantaneously attained.

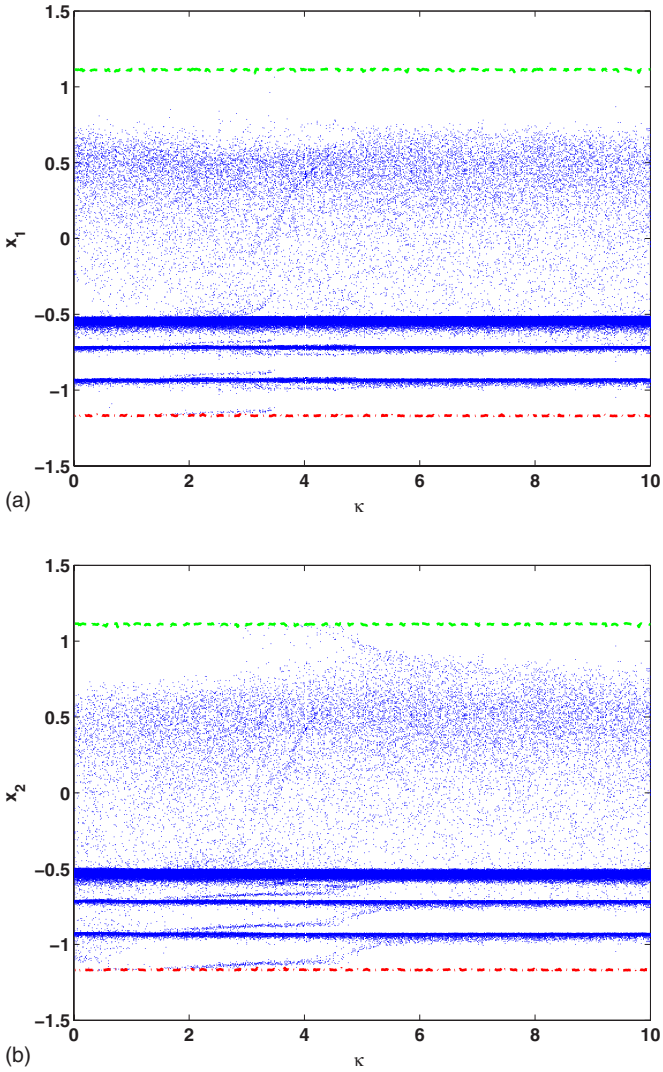

FIG. 6. (Color online) As in Fig. 4 but for another sample of amplitudes $A_1=0.721$, $A_2=0.724$ and phases $\phi_1^0=1.494$ and $\phi_2^0=1.649$.

To explore how heterogeneity in the parameters of the driving forces influences the synchronization features we show in Fig. 9 the degree of synchrony versus the coupling strength and the difference of either the drivers' amplitudes A_1-A_2 or phases $\phi_1^0-\phi_2^0$, respectively. The graphs are gen-

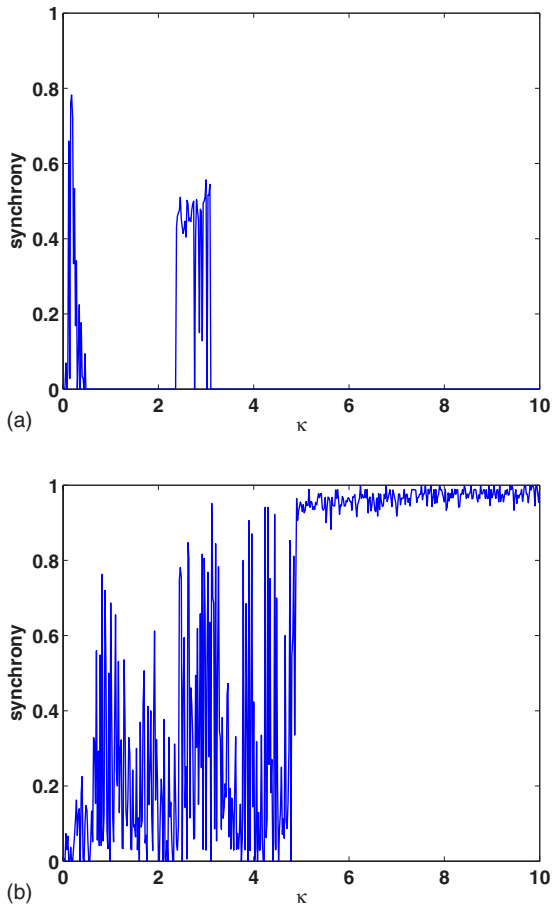

FIG. 7. (Color online) Degree of synchronization as a function of the coupling strength κ. Remaining parameters as in Figs. 4 (a) and 6 (b).

erated by integrating the coupled dynamics for 1000 realizations of random amplitudes and phases and at the end of the simulation time for every sample the degree of synchrony is plotted. The graphs possess reflection symmetry with respect to the lines $\phi_1^0-\phi_2^0=0$ and $A_1-A_2=0$, respectively. For couplings $\kappa\lesssim 4$ in a broad range of amplitude and phase differences the coupled dynamics attains a synchronized state of fairly weak degree of synchrony. For larger coupling strengths synchronization is realized only in confined ranges of the amplitude and phase differences. This is mainly due to the raising number of events of firing death. For strong coupling the major contribution to the pronounced synchrony stems from small phase differences $|\phi_1^0-\phi_2^0|$ being attributed to the fairly broad central tongue in Fig. 9. There occur gaps associated with asynchrony at intermediate phase differences while thin tongues corresponding to strong synchrony result at phase differences for which ϕ_1^0 is close to 2π and $\phi_2^0\simeq 0$ or vice versa, viz., the two driving forces act almost in phase. Equivalent behavior is reflected in the graph of synchrony versus the amplitude difference A_1-A_2 and the coupling strength. The left, central, and right tongue in Fig. 9(b) belong to their respective counterpart in Fig. 9(a). Incidentally, the amplitude and phase differences for the example illustrated in Figs. 4 and 6 fall into one of the gaps of asynchrony and tongues of synchrony respectively which occur at large coupling strengths in Fig. 9.

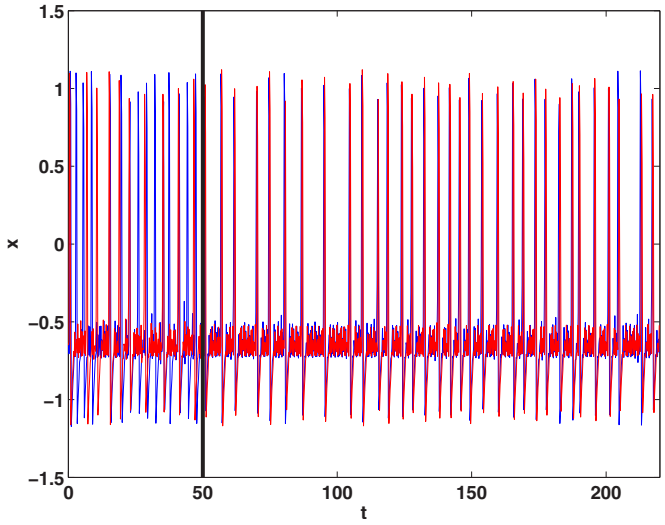

FIG. 8. (Color online) Example of chaotic synchronization of two FHN units. In the interval $0\leq t<50$ the units are uncoupled, i.e., $\kappa=0$. The vertical line at $t=50$ indicates the moment of the switch-on of the coupling of strength $\kappa=5$. Remaining parameters as in Fig. 7(b).

3. Phase coherence

Spike synchronization necessitates that at least during the periods of firing activity the phases of the FHN units are

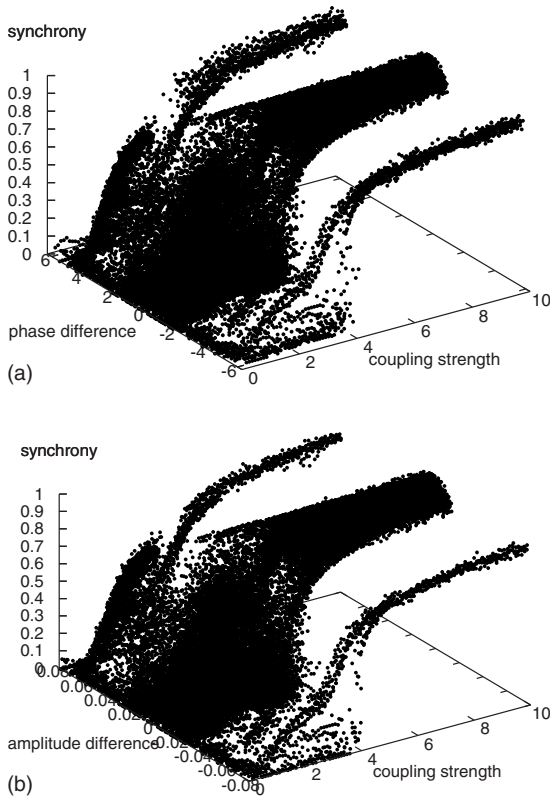

FIG. 9. Degree of synchrony as a function of the coupling strength κ and the phase (amplitude) difference $\phi_1^0-\phi_2^0$, (A_1-A_2) in (a) [(b)] where $\phi_{1,2}^0\in[0,2\pi)$ and $A_{1,2}\in[0.70,0.79]$. White areas correspond to complete asynchrony.

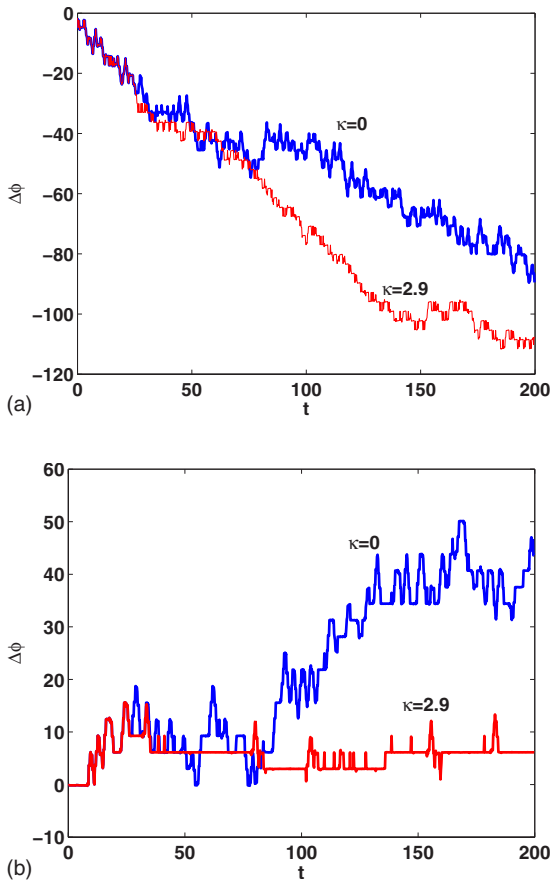

FIG. 10. (Color online) Temporal behavior of the phase difference $\Delta\phi$. (a) [(b)] Parameters as in Figs. 4 and 6 except for the values of the coupling strength as indicated in the plot.

synchronized. It is illuminative to consider in the following the dynamics of the phases which serves especially to understand the ramification of the phase difference $\Delta\phi^0=\phi_1^0-\phi_2^0$ on the onset of spike synchronization. To this end we introduce the angle variable $\phi_{1,2}(t)$ which can be treated as an estimate of the phase variable [42,43] for rotations around the stable fixed point (x_0,y_0) in the $x-y$ plane. Shifting the origin of the plane to (x_0,y_0) and passing to polar coordinates we define

$$\phi_{1,2}(t)=\tan^{-1}[x_{1,2}(t)/y_{1,2}(t)]. \tag{22}$$

In Fig. 10 the time evolution of the phase difference $\Delta\phi(t)=\phi_1(t)-\phi_2(t)-\Delta\phi^0$ is depicted with amplitudes $A_{1,2}$ and phases $\phi_{1,2}^0$ taken from the two examples of Figs. 4 and 6. In the former case we notice low degree of synchrony for small κ and firing death for big κ while in the latter case even complete chaotic synchronization results for strong coupling (see also Fig. 7). For $\kappa=0$ the phase difference grows in the course of time in both cases. For rather big stimulus phase difference $\Delta\phi^0=-1.621$ [(a)] the phase difference of the signal $\Delta\phi(t)$ grows on the average almost linearly. In comparison for a small stimulus phase difference $\Delta\phi^0=-0.016$ [(b)] the growth is not as pronounced as in the previous case. Moreover, temporarily the signal phase difference essentially does not grow and rather oscillates irregularly around a plateau. When coupled with strength $\kappa=2.9$ the phase differences behave completely different. The coupling is switched on at $t=25$. In the case of rather big $\Delta\phi^0=-1.621$ [(a)] for the phase difference $\Delta\phi(t)$ still unbounded growth is obtained and the firings of the two FHN units evolve accordingly asynchronously (see Fig. 4). For a small value of $\Delta\phi^0=-0.016$ [(b)] extended intervals of phase entrainment result which are interrupted by occasional sudden up-and-down jumps. Most importantly, in the last case the (partial) phase synchronization is connected with spike synchronization (see Fig. 6) albeit with a rather low degree of synchrony of 0.249. The histograms of the phase difference taken modulo 2π are shown in Fig. 11. For inhibited synchronization features corresponding to the behavior shown in Fig. 10(a) the distribution of the phase difference exhibits a maximum around an intermediate value 0.3 whereas in the case for which synchronization is supported [see Fig. 10(b)] the distribution of the phase difference has a pronounced maximum near zero and two smaller peaks around π. For stronger couplings $\kappa>2.9$ phase synchronization gets improved compared to the behavior in Fig. 10 and eventually as a result of strong enough coupling complete phase synchronization is observed so that the degree of synchrony is enhanced too.

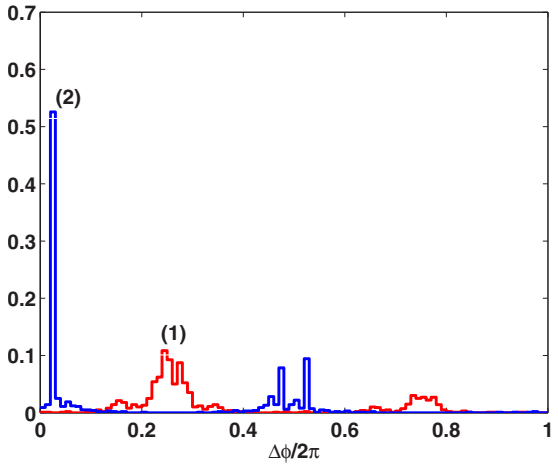

FIG. 11. (Color online) Histograms of the phase difference $\Delta\phi/2\pi$ for the coupled dynamics with $\kappa=2.9$. The label (1) corresponds to the behavior marked with $\kappa=2.9$ in Fig. 10(b) and label (2) to those marked with $\kappa=2.9$ in Fig. 10(a).

In the case of driving with only random amplitudes but fixed phase strong synchrony yields irrespective of the amplitude heterogeneity for large coupling strengths as seen in Fig. 12. In particular we do not notice events of firing death.

4. Statistical properties of spiking sequences

In order to characterize the variability of spiking sequences (interspike intervals) we compute the coefficient of variation CV and the firing rate ρ [44]. Denoting with $t_0^{(i)}<t_1^{(i)}<\cdots<t_{K_i}^{(i)}$ series of firing times of x_i the interspike intervals are defined as $T_k^{(i)}=t_k^{(i)}-t_{k-1}^{(i)}$ $(k=1,2,\ldots,K_i)$. The coefficient of variation is given by

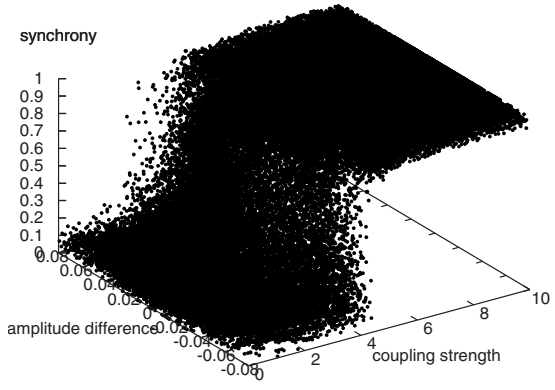

FIG. 12. Degree of synchrony as a function of the coupling strength κ and the amplitude difference A_1-A_2 for forcing with random amplitudes $A_{1,2}\in[0.70,0.79]$ and fixed phase $\phi_n^0=0$.

$$CV=\frac{\sqrt{\langle (T_k^{(i)})^2\rangle-\langle T_k^{(i)}\rangle^2}}{\langle T_k^{(i)}\rangle}, \tag{23}$$

with

$$\langle (T_k^{(i)})^n\rangle=\frac{\sum_{i=1,2}\sum_{k=1}^{K_i}(T_k^{(i)})^n}{\sum_{i=1,2}K_i}. \tag{24}$$

For a strictly periodic process the CV is zero and hence, the smaller the CV the more coherent the spike sequence.

The firing rate of a unit is defined as the average frequency of firing during one period T of the external driving

$$\rho=\frac{TM}{\sum_{n=1}^{M}T_n}, \tag{25}$$

where M and T_n denote the number of periods and the nth interspike interval of the considered unit, respectively. The mean degree of synchrony, the coefficient of variation and the firing rate computed as the average over 500 samples with random values of phases and/or amplitudes of the driving force as a function of the coupling strength are illustrated in Fig. 13. In the case of randomly distributed amplitudes but equal phases of the driving terms enlarging the coupling strength leads to rather rapidly and monotonically growing degree of synchrony up to a value 0.8 in the coupling range $0<\kappa\lesssim 6.2$. Upon further increase of κ synchrony rises only weakly.

In the other case, namely, random amplitudes together with random phases increasing the coupling up to $\kappa\lesssim 1$ improves more rapidly synchrony than in the previous case. For $\kappa>1$ there follow a break down and an interlude of nearly constant low synchrony at the end of which at $\kappa\simeq 4.2$ with little further increase of κ the synchrony steeply rises again to a maximum value. However, enlarging κ beyond the value 6 results in slow but gradual decline of synchrony. This shows that for high amount of heterogeneity strengthening the coupling does not necessarily entail better synchrony and

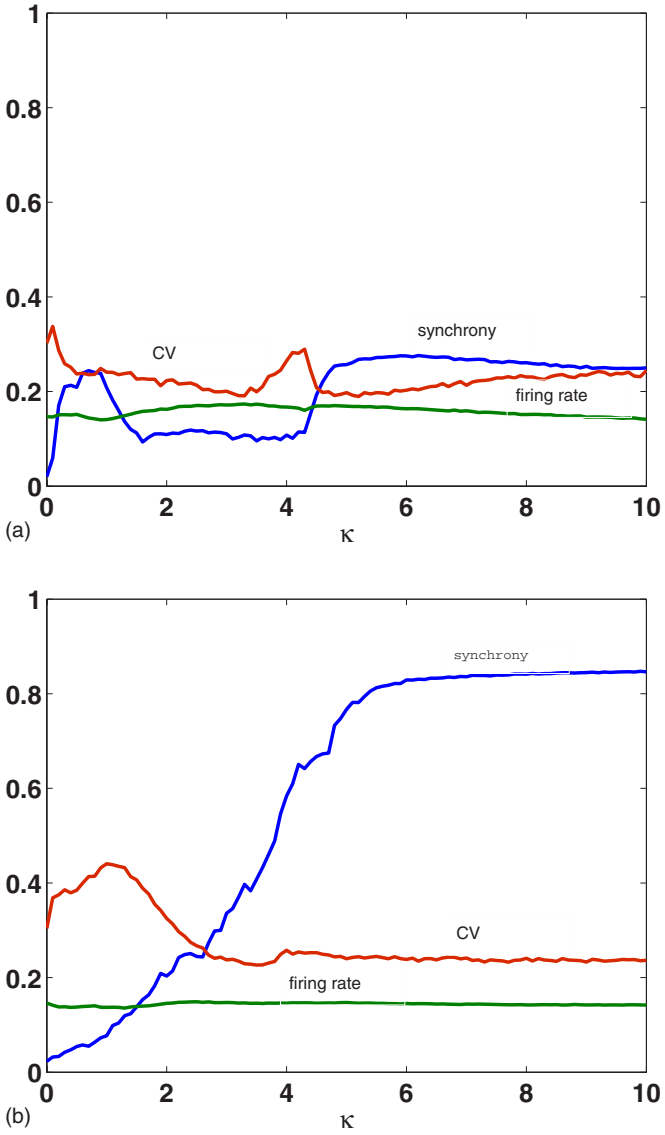

FIG. 13. (Color online) Mean degree of synchrony CV and firing rate of the first unit ρ [defined in Eqs. (23) and (25), respectively] as labeled in the plot as a function of the coupling strength κ. (a) Driving with random amplitudes and random phases evenly distributed in the interval $A_{1,2}\in[0.7,0.79]$ and $\phi_{1,2}^0\in[0,2\pi)$, respectively. (b) Driving with random amplitudes and fixed phase $\phi_{1,2}^0=0$. Remaining parameters as in Fig. 7.

rather the opposite is true. Interestingly in the weak coupling range $\kappa\lesssim 1$ strong heterogeneity in the forcing, viz., with random amplitudes and phases, sustains better synchrony than driving with random amplitudes but constant phase.

We remark that for the case of forcing with fixed amplitude taken from the interval [0.70, 0.79] and random phases (not shown here) we obtain results that are similar to the ones of driving with random amplitudes and random phases. Hence, the phase relation between the driving terms crucially governs the ability to synchronize the spiking events. We underline that even if the two units fail to completely synchronize their firing events, they nonetheless might become mutually amplitude-locked to subthreshold oscillations

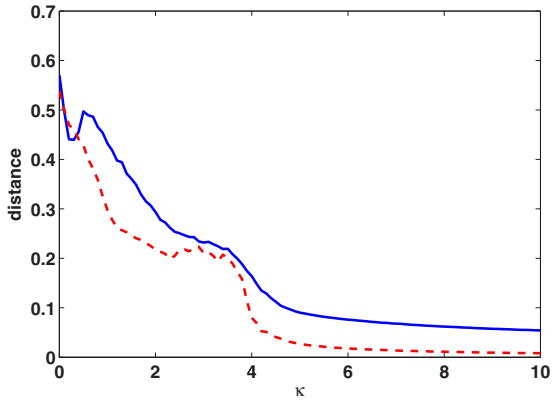

FIG. 14. (Color online) Mean distance between the trajectories of the two units as a function of the coupling strength. Averages were performed over 500 realizations of random values for the amplitudes and phases. Blue solid line: Random amplitudes and random phases. Red dashed line: Random amplitude and fixed phase $\phi^0=0$. Parameters as in Fig. 13.

though as it is, e.g., the case illustrated in Fig. 4(a) for strong enough coupling.

For driving with random amplitudes but fixed phase the *CV* grows monotonically for low couplings reaching a maximum at $\kappa \simeq 1.7$ [see Fig. 13(b)]. With further enlarged κ the *CV* drops and settles eventually for $\kappa \simeq 5$ on a plateau. In contrast to that is the behavior of the *CV* in the case of forcing with random amplitudes and random phases [see Fig. 13(a)]. Here the *CV* is even lowered with increasing coupling until $\kappa \lesssim 3.5$ apart from the small growth for $\kappa \ll 1$. In the range $3.5 \lesssim \kappa \lesssim 4.5$ there follows a stage of sudden rise and subsequent fall of the *CV* and for $\kappa \gtrsim 5$ the *CV* weakly grows but notably, stays below the corresponding values found for driving with random amplitude and fixed phase. Conclusively, the trend to more enhanced chaotic synchronization upon enlarging the coupling strength is not necessarily connected with higher regularity in the corresponding spike trains compared to the irregularity in the spike trains of weaker synchronized states. Different behavior was observed for two coupled Hindmarsh-Rose neurons where the complexity of the time-interval sequences gets simpler the stronger the coupling [41].

The firing rate does not exhibit a pronounced dependency on the coupling strength and hence, the mean length of the (irregularly distributed) interspike intervals is more or less insensitive to changes of κ. The attainment of complete synchrony with increasing coupling strength is also confirmed by a gradually diminishing mean distance between the trajectories of the two units

$$\bar{d} = \frac{1}{N}\sum_{n=1}^{N} \sqrt{(x_n - x_{n-1})^2 + (y_n - y_{n-1})^2}, \tag{26}$$

as is seen in Fig. 14. Already for $\kappa=10$ the distance between the two trajectories has shrunk significantly and if the coupling strength is increased toward the one predicted by the theorem in Sec. II the distance further diminishes so that complete synchronization is indeed achieved. We remark that

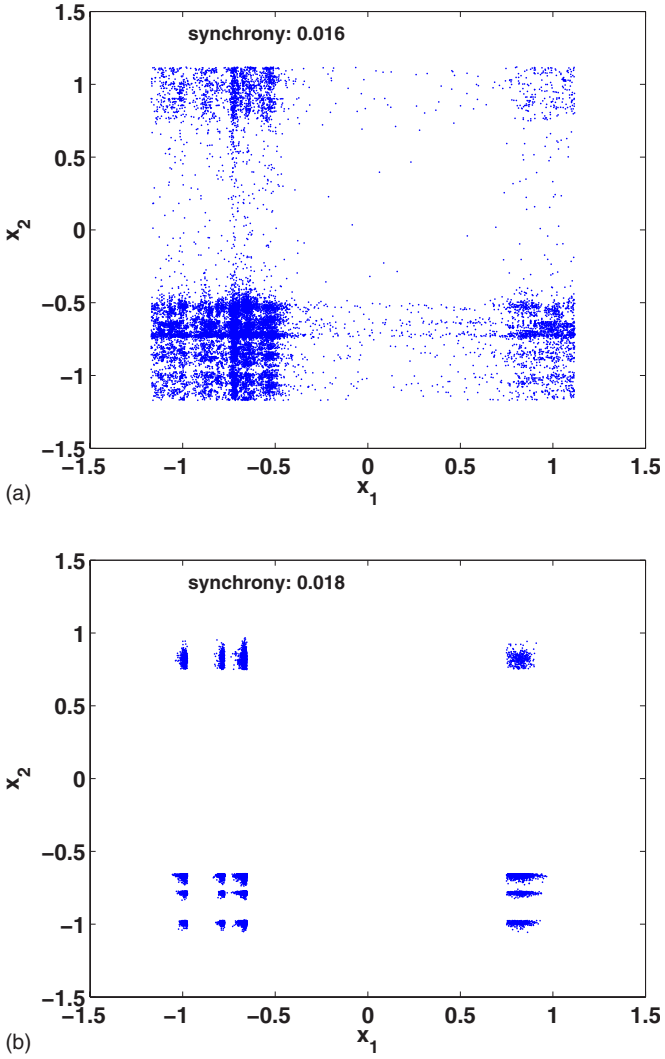

FIG. 15. (Color online) Projection of the attractor: Stroboscopic plot of the dynamics in the uncoupled limit. (a) [(b)] Random (fixed) phases. The evolution of an ensemble of 500 systems is superimposed on one plane and the respective synchrony measure is indicated in the figure. Parameters as in Fig. 13.

the coupling strengths $\kappa \leq 10$ considered in this work are still small compared to the coupling strength that guarantees according to the theorem in Sec. II complete synchronization. The latter value is of the order of $\kappa \gtrsim 100$. The synchronization features are conveniently summarized by projecting stroboscopic plots of the dynamics onto the x_1-x_2 plane. In Figs. 15 and 16 the dynamics of an ensemble of 500 samples of random amplitudes and/or phases are superimposed on one plane. In addition the corresponding synchronization measure is indicated in the plots. As Fig. 15 reveals with random phases the projection of the attractor of the uncoupled dynamics provides a widespread pattern of points that are scattered all over the plane attributed to noncoherent evolution of the two subsystems [see Fig. 15(a)]. When the phases are fixed the attractor consists of several groups of clouds that altogether occupy less area on the plane compared to the previous case [see Fig. 15(b)]. Two groups of the clouds are distributed around the main and secondary diago-

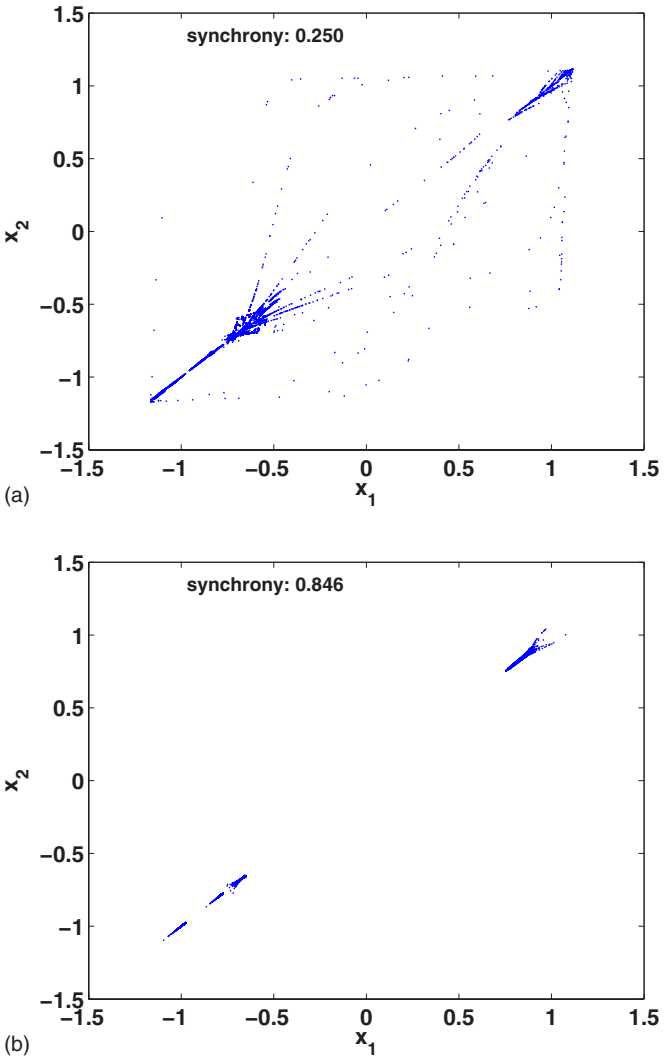

FIG. 16. (Color online) As in Fig. 15 except for the coupling strength $\kappa=10$.

nal respectively indicating that there exists coupled dynamics being not too far from in-phase and out-of-phase motion of the activators, respectively.

With switched on strong coupling the dynamics is triggered in the regime of coherent motion. Especially in the case of fixed phases and random amplitudes virtually all points come to lie on the main diagonal being associated with full synchrony [see Fig. 16(b)]. In comparison random phases lead to an attractor that, apart from few points, is confined to the neighborhood of the main diagonal. However, pronounced synchronization is inhibited as indicated by the synchronization measure in the figure [see Fig. 16(a)].

IV. SUMMARY

We have investigated the synchronization properties of two coupled FHN units in an excitable regime. Interest is focused on the response of the interacting units to heterogeneous external inputs. Imposing the inhibitor variable of each FHN unit to a periodic and parametric force chaotic firing events are generated. Furthermore, due to random choices of the amplitudes and/or phases of the two external forces the firings of the units occur mutually asynchronous for the uncoupled dynamics.

When the coupling between the two units is turned on we have observed that for low amount of heterogeneity, viz., for driving with only dispersed amplitudes but equal phases, the degree of synchrony gets enhanced with growing coupling strength. Despite the improvement of synchrony upon enlarging the coupling strength the spiking sequence (interspike interval) remains irregular though which is reflected in a fairly large coefficient of variation. This has to be differentiated from the results in Ref. [41] concerning the irregular dynamics of two coupled neurons where the complexity of the time-interval sequences gets the more regular the stronger the coupling is.

In clear contrast, for higher amount of heterogeneity, that is forcing with dispersed amplitudes together with dispersed phases, the degree of synchrony cannot be improved beyond a certain maximal degree by enlarging the coupling strength. Moreover, if the difference between the phases and/or the amplitudes of the tow driving forces exceeds a critical value synchrony is excluded for too strong couplings. In the latter case we have found that the coupled units annihilate mutually their firings due to a coupling-induced modification of the excitation threshold. We call this phenomenon "firing death" in accordance with the effect known as oscillation death, occurring when units of oscillatory networks reciprocally annihilate their oscillations for overcritical coupling strength [35]. Nevertheless in the absence of synchrony the units perform completely synchronous subthreshold oscillations for strong enough coupling as it is also confirmed by our corresponding synchronization theorem.

ACKNOWLEDGMENTS

This research was supported by SFB 555 and the VW Foundation Project I/80425.

[1] Y. Kuramoto, *Chemical Oscillations, Waves, and Turbulence* (Springer, Berlin, 1984).
[2] J. D. Murray, *Mathematical Biology* (Springer, New York, 1993).
[3] A. Pikovsky, M. Rosenblum, and J. Kurths, *Synchronization* (Cambridge University Press, Cambridge, UK, 2001).
[4] S. H. Strogatz, C. M. Marcus, R. M. Westervelt, and R. E. Mirollo, Phys. Rev. Lett. **61**, 2380 (1988).
[5] A. T. Winfree, *The Geometry of Biological Time* (Springer, New York, 1980).
[6] J. A. S. Keslo, *Dynamic Patterns: The Self-Organization of Brain and Behavior* (MIT Press, Cambridge, MA, 1995).

[7] C. M. Gray, P. König, A. K. Engel, and W. Singer, Nature (London) **338**, 334 (1989).
[8] M. Bazhenov, M. Stopfer, M. Rabinovich, R. Huerta, H. D. I. Abarbanel, T. J. Sejnowski, and G. Laurent, Nature (London) **30**, 553 (2001).
[9] C. Meunier and I. Segev, in *Neuro-Informatics and Neural Modelling*, edited by F. Moss and S. Gielen (North-Holland, Amsterdam, 2001), p. 353.
[10] D. Hansel and H. Sompolinsky, Phys. Rev. Lett. **68**, 718 (1992).
[11] J. J. Hopfield, Nature (London) **376**, 33 (1995).
[12] J. C. Eccles, *The Understanding of the Brain* (McGraw-Hill, New York, 1973).
[13] R. FitzHugh, Biophys. J. **1**, 445 (1961); J. Nagumo, S. Arimoto, and S. Yoshizawa, Proc. IRE **50**, 2061 (1962).
[14] F. C. Hoppensteadt, *An Introduction to the Mathematics of Neurons* (Cambridge University Press, New York, 1986).
[15] A. L. Hodgkin and A. F. Huxley, J. Physiol. **117**, 500 (1952).
[16] B. Van der Pol, Philos. Mag. **30**, 64 (1927).
[17] J. Guckenheimer and P. Holmes, *Nonlinear Oscillation, Dynamical Systems, and Bifurcation of Vector Fields* (Springer, New York, 1986).
[18] G. Matsumoto, K. Aihara, M. Ichikawa, and A. Tasaki, J. Theor. Neurobiol. **3**, 1 (1984).
[19] K. Aihara, G. Matsumoto, and Y. Ikegaya, J. Theor. Biol. **109**, 249 (1984).
[20] G. Matsumoto, K. Aihara, Y. Hanyu, N. Takahashi, S. Yoshizawa, and J. Nagumo, Phys. Lett. A **123**, 162 (1987).
[21] M. Feingold, D. L. González, O. Piro, and H. Viturro, Phys. Rev. A **37**, 4060 (1988).
[22] D. T. Kaplan, J. R. Clay, T. Manning, L. Glass, M. R. Guevara, and A. Shrier, Phys. Rev. Lett. **76**, 4074 (1996).
[23] T. Yanagita, Y. Nishiura, and R. Kobayashi, Phys. Rev. E **71**, 036226 (2005).
[24] L. Glass, Nature (London) **410**, 277 (2001); M. Braune and H. Engel, Chem. Phys. Lett. **211**, 534 (1993); O. Steinbock, V. Zykov, and S. C. Müller, Nature (London) **366**, 322 (1993); A. Karma and V. S. Zykov, Phys. Rev. Lett. **83**, 2453 (1999); W. J. Yeh, D. R. He, and Y. H. Kao, *ibid.* **52**, 480 (1984).
[25] H. Fujii and I. Tsuda, Lect. Notes Comput. Sci. **3146**, 140 (2004).
[26] V. E. Bondarenko and T. R. Chay, Phys. Rev. E **58**, 8036 (1998).
[27] K. Tateno, H. Tomonari, H. Hayyashi, and S. Ishizuka, Int. J. Bifurcation Chaos Appl. Sci. Eng. **14**, 1559 (2004).
[28] Yu. Shinohara, T. Kanamaru, H. Suzuki, T. Horita, and K. Aihara, Phys. Rev. E **65**, 051906 (2002).
[29] J. H. E. Cartwright, Phys. Rev. E **62**, 1149 (2000).
[30] L. M. Pecora and T. L. Carroll, Phys. Rev. Lett. **80**, 2109 (1998); L. M. Pecora, Phys. Rev. E **58**, 347 (1998).
[31] V. N. Belykh, I. V. Belykh, and M. Hasler, Physica D **195**, 159 (2004).
[32] L. M. Pecora and T. L. Carroll, Phys. Rev. Lett. **64**, 821 (1990).
[33] M. G. Rosenblum, A. S. Pikovsky, and J. Kurths, Phys. Rev. Lett. **76**, 1804 (1996).
[34] M. Dhamala, V. K. Jirsa, and M. Ding, Phys. Rev. Lett. **92**, 028101 (2004).
[35] E. Rossoni, Y. Chen, M. Ding, and J. Feng, Phys. Rev. E **71**, 061904 (2005); K. Bar-Eli, Physica D **14**, 242 (1985); D. G. Aronson, G. B. Ermentrout, and N. Kopell, *ibid.* **41**, 403 (1990); R. E. Mirollo and S. H. Strogatz, J. Stat. Phys. **60**, 245 (1990); Y. Yamaguchi and H. Shimizu, Physica D **11**, 212 (1984); T. Nomura and L. Glass, Phys. Rev. E **53**, 6353 (1996); C. G. Assisi, V. K. Jirsa, and J. A. Scott Kelso, Phys. Rev. Lett. **94**, 018106 (2005).
[36] A. W. Przybyszewski, M. J. M. Lankheet, and W. A. van de Grind, Biol. Cybern. **74**, 299 (1996); C. D. Boschi, E. Louis, and G. Ortega, Phys. Rev. E **65**, 012901 (2001); P.-L. Gong and J.-X. Xu, *ibid.* **63**, 031906 (2001); A. L. Lin, A. Hagberg, E. Meron, and H. Swinney, *ibid.* **69**, 066217 (2004); G. Zhao, Z. Hou, and H. Xin, Phys. Chem. Chem. Phys. **7**, 3634 (2005); B. Marts, A. Hagberg, E. Meron, and A. Lin, Chaos **16**, 037113 (2006).
[37] L. Meinhold and L. Schimansky-Geier, Phys. Rev. E **66**, 050901(R) (2002); Y. I. Balkarey, V. O. Nagoutchev, M. G. Evtikhov, and M. I. Elinson, Neural Process. Lett. **12**, 215 (2000); J. W. Shuai and P. Jung, Phys. Rev. Lett. **88**, 068102 (2002); Biophys. J. **83**, 87 (2002); E. Ullner, A. Zaikin, J. García-Ojalvo, and J. Kurths, Phys. Rev. Lett. **91**, 180601 (2003).
[38] W. Eckhaus, *Lecture Notes in Mathematics* (Springer-Verlag, Berlin, 1983); F. Dumortier and R. Roussarie, Mem. Am. Math. Soc. **121**, 577 (1996); M. Krupa and P. Szmolyan, J. Differ. Equations **174**, 312 (2001).
[39] J. A. White, C. C. Chow, J. Ritt, C. Soto-Treviño, and N. Koppel, J. Comput. Neurosci. **5**, 5 (1998).
[40] X.-J. Wang and G. Buzsaki, J. Neurosci. **16**, 6402 (1996).
[41] W. Wang, G. Perez, and H. A. Cerdeira, Phys. Rev. E **47**, 2893 (1993).
[42] A. Goryachev and R. Kapral, Phys. Rev. Lett. **76**, 1619 (1996).
[43] A. Pikovsky, M. Rosenblum, and J. Kurths, Europhys. Lett. **34**, 165 (1996).
[44] B. Lindner, J. García-Ojalvo, A. Neiman, and L. Schimansky-Geier, Phys. Rep. **392**, 321 (2004).